

# Behavior of CFRP Strengthened Reinforced Concrete Beams in Corrosive Environment

Khaled Soudki<sup>1</sup>; Ehab El-Salakawy<sup>2</sup>; and Brent Craig<sup>3</sup>

**Abstract:** This paper reports the test results of 11 reinforced concrete beams strengthened with carbon fiber-reinforced polymer (CFRP) sheets and subjected to an aggressive environment. In this study, eight beams were cracked and repaired with CFRP sheets, while the remaining three beams were kept uncracked as a control. The beams were 150 mm wide by 250 mm deep by 2,400 mm long and lightly reinforced with a reinforcement ratio of 0.6%. Two types of carbon FRP products were considered: Sheets and strips. In terms of environmental exposure, three beams were kept at room temperature and eight beams were subjected up to 300 wetting and drying cycles with deicing chemicals (3% NaCl). Following the exposure, the beams were tested to failure in four-point bending. In addition, nondestructive tests were performed to determine the corrosion rate, as well as destructive tests to determine chloride diffusion and reinforcing bar mass loss. Based on the findings of the study, the long-term effectiveness of the CFRP strengthened reinforced concrete in aggressive corrosive environments was established.

**DOI:** 10.1061/(ASCE)1090-0268(2007)11:3(291)

**CE Database subject headings:** Concrete, reinforced; Durability; Rehabilitation; Composite materials; Carbon; Glass; Cycles; Beams.

## Introduction

Fiber-reinforced polymer (FRP) reinforcement is increasingly becoming prominent in the strengthening and rehabilitation of reinforced concrete (RC) structures. Strengthening techniques using FRPs involve the external bonding of laminates to concrete slabs and beams, or the wrapping of concrete columns. Interest in these techniques is widespread, and continues to grow, due to the ease of installation, lower cost, negligible clearance loss, and high strength to weight ratio of FRP materials. Numerous studies (Spadea et al. 1998; Matthys 2000; ACI Committee 440 2002; Tamuzs and Tepfers 2004) have shown that concrete rehabilitation using FRPs is very successful at restoring or increasing the strength of concrete members. The basic concepts in the use of FRPs for strengthening of concrete structures are covered in a review article by Triantafyllou (1998). Progress in various strengthening methods, questions associated with the long-term durability of FRP, as well as the development of design guidelines and codes are addressed in a review paper by Neale (2000). A further aspect of the FRP rehabilitation that shows promise is the

prevention of chloride ion ingress into concrete. The use of carbon FRP (CFRP) laminates as a means to delay corrosion damage in concrete is being investigated in this research study. The objective of this paper is to present the results on the durability performance of CFRP strengthened reinforced concrete beams subjected to wet-dry cycles in the presence of deicing chemicals.

Much research has been done on structural members wrapped with CFRP fabric and subjected to wet-dry cycles (Chajes et al. 1995; Toutanji and Balaguru 1998; Spainhour and Thompson 1998; Mohammed et al. 2003). The previous work mainly focused on small-scale experiments (beams or columns). There is a lack of experimental data on larger-scale specimens. To the best knowledge of the writers, prior to the recent work of Spainhour and Thompson (1998), no one has addressed the effect of wet-dry cycles on rebar corrosion, chloride content, and the structural behavior of specimens wrapped with CFRP fabrics.

The present research aims to provide insight into this area by exposing the larger-scale reinforced concrete (RC) beams wrapped with CFRP fabric or strips to an aggressive environment. The objectives are to validate the efficiency of CFRP strengthening in aggressive environments, such as wetting and drying in the presence of salts; to obtain corrosion measurements using field equipment for such members; and to quantify how CFRP wrapping will reduce the rate of corrosion activity in reinforced concrete.

## Test Program

Table 1 summarizes the experimental program. A total of 11 reinforced concrete beams are used: 8 beams are cracked and strengthened with CFRP sheets, while the remaining 3 beams are kept uncracked as a control. The beams were initially precracked at service load and strengthened with CFRP laminates in the unloaded condition. Each beam specimen was 2.40 m long with a

<sup>1</sup>Professor, Canada Research Chair, Dept. of Civil Engineering, Univ. of Waterloo, Waterloo, Ontario, Canada N2L 3G1. E-mail: soudki@uwaterloo.ca

<sup>2</sup>Associate Professor, Canada Research Chair, Dept. of Civil Engineering, Univ. of Manitoba, Winnipeg, Canada R3T 5V6. E-mail: ehab.elsalakawy@usherbrooke.ca

<sup>3</sup>Structural Engineer, Acres International, 4342 Queen St., Niagara Falls, Ontario, Canada L2E 6W1.

Note. Discussion open until November 1, 2007. Separate discussions must be submitted for individual papers. To extend the closing date by one month, a written request must be filed with the ASCE Managing Editor. The manuscript for this paper was submitted for review and possible publication on November 25, 2002; approved on December 22, 2005. This paper is part of the *Journal of Composites for Construction*, Vol. 11, No. 3, June 1, 2007. ©ASCE, ISSN 1090-0268/2007/3-291-298/\$25.00.

**Table 1.** Test Program

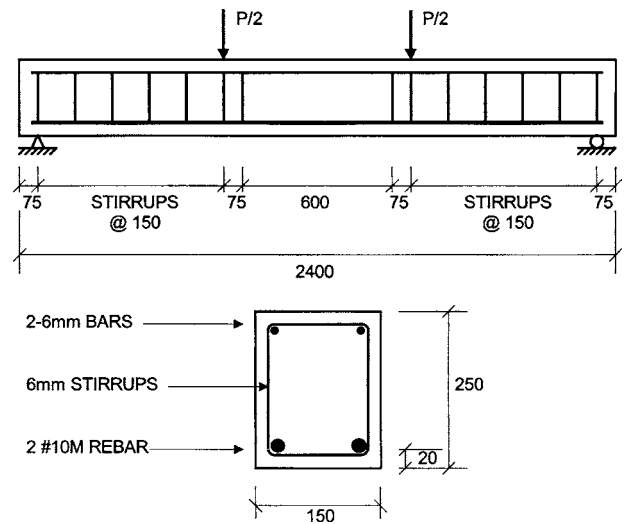
Strengthening scheme	Wet/Dry cycles			
	0	100	200	300
Control (unstrengthened)	C-0	C-100	—	C-300
Forca-tow sheet	T-0	T-100	T-200	T-300
CarboDur strip	S-0	S-100	S-200	S-300

120 × 175 mm rectangular cross section and reinforced with two No. 10 M bottom longitudinal deformed reinforcing bars (reinforcement ratio of 0.6%), two 6-mm-diameter top longitudinal plain reinforcing bars, and 6-mm-diameter plain stirrups spaced at 150 mm. A typical clear cover of 20 mm was used all around the stirrups. Fig. 1 shows the reinforcement details of the test specimen.

The 28-day compressive strength of the concrete used was on average 35 MPa. The laboratory obtained yield stress and strain of the tension steel reinforcing bars were 460 MPa and 0.2%, respectively. Based on the test setup (four-point bending), the design flexural capacity of the control (unstrengthened) beam is approximately one-third of its shear capacity.

Two types of CFRP products were considered: Forca-Tow sheets (FTS-C1-20) manufactured by Forca-Tow Corp., Japan; and CarboDur S512 strips manufactured by Sika, Canada. The mechanical properties of the carbon fibers and the composite CFRP sheets for both Forca-Tow sheets and CarboDur strips are shown in Table 2 (taken from the manufacturer data sheets). Table 2 lists the mechanical properties of the carbon fibers in their dry condition, and the mechanical properties of the cured composite CFRP sheet that includes the combined effect of fibers and resin after curing, which should be used for design purposes. The cured thickness of the Forca-Tow sheets range from 0.6 to 1.0 mm. The strengthening schemes are demonstrated in Fig. 2.

Strengthening Scheme I uses one CFRP CarboDur strip (50 mm width × 1.2 mm thick) bonded to the bottom face for the entire beam length. In addition, a 200 mm region of the beam by the supports was wrapped with a layer of CFRP Sika-Wrap Hex-103C sheets (manufactured by Sika, Canada) running transversely around the cross section of the beam [Fig. 2(c)]. These transverse CFRP sheets provide anchorage for the longitudinal plate against premature debonding, and prevent any premature failure that might happen in the concrete cover between the CFRP strip and the longitudinal steel. Strengthening Scheme II uses four layers of the Forca-Tow sheets (each layer is 0.11 mm thick in dry fiber condition) to strengthen the entire span of the beam. One layer of U-shaped Forca-Tow CFRP strips [90 mm wide—Fig. 2(d)] with the fibers oriented in the transverse direction were bonded around the cross section throughout the beam length to provide sufficient

**Fig. 1.** Test specimen reinforcement configuration

anchorage and to prevent the longitudinal sheets from locally peeling off. It should be noted here that the beams strengthened with this scheme were totally coated with epoxy all over three surfaces, bottom, and two sides.

In terms of environmental exposure, three beams were kept in a normal lab environment (around 25 °C and 30% relative humidity) and eight beams were subjected to wetting and drying cycles (100, 200, and 300 cycles) in the presence of deicing chemicals (3% NaCl) at room temperature. The wet-dry cycle took 2 days, which consisted of wetting the beams for 1 day followed by 1 day of drying. The setup for the wet-dry cycles can be seen in Fig. 3. It should be noted that there are no standard test methods for the wet-dry cycle exposure. The cyclic regime followed and the number of cycles chosen to achieve the active corrosion in a reasonable time span (300 cycles or 600 days). Following the environmental exposure, two nondestructive tests were performed: Electrical potential measurements and corrosion rate measurements. Specimens were then tested under monotonic load until failure. The specimens were tested in four-point bending over a 2,250 mm simply supported span. The two point loads were positioned at one-third span length, and loading was under displacement control as shown in Fig. 4. The static load was incremented gradually until failure occurred. The beam deflection was measured at the midspan by means of a linear variable differential transducer. Concrete strains were recorded at the midspan. At the top face, 60-mm long electrical strain gauges were used. At the side face, demec points over a gauge length of 200 mm were used. Electrical strain gauges of 5-mm gauge length were at-

**Table 2.** Mechanical Properties of Carbon Fibers and Composite Sheets<sup>a</sup>

Type	Thickness (dry fibers) (mm)	Carbon fiber properties (dry fibers)		Composite sheet properties (fibers + resin)		
		Ultimate strength (MPa)	Modulus of elasticity (GPa)	Ultimate strength/1 m width (kN)	Axial stiffness (MN m)	Elongation at break (%)
Sika CarboDur S512 <sup>b</sup>	1.20	2,800	165	N/A	N/A	1.7
Forca-Tow FTS-C1-20	0.11	3,480	230	385	25.3	1.5

<sup>a</sup>Taken from the manufacturers' technical data sheets.

<sup>b</sup>Has unique properties since carbon fiber is encapsulated in a precured laminate (strip).

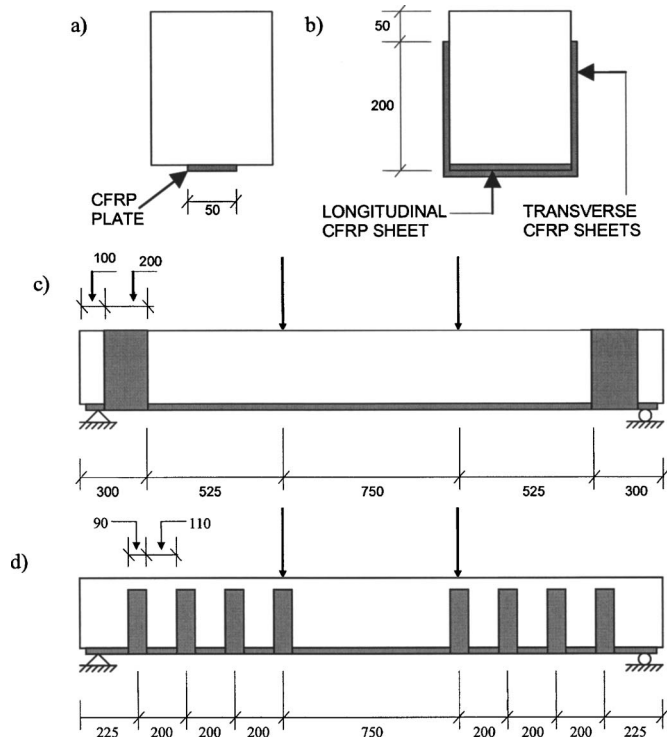


**Fig. 2.** Schematic of strengthening schemes: (a) and (c) Scheme I with CarboDur strips; (b) and (d) Scheme II with Forca Tow sheets

tached on the tension steel and also on the FRP strips and the sheets to measure the strain behavior. All instrumentation were computer controlled and automatically logged the data.

## Test Results and Discussions

### Monitoring Corrosion Activity

The corrosion activity within the specimens was monitored using nondestructive and destructive techniques during the aggressive environmental exposure. The nondestructive techniques included half-cell potential measurements and corrosion rate measurements. The destructive techniques, performed after load testing of the specimens to failure, included chloride profiling and mass loss analysis. The following presents the results of these tests.

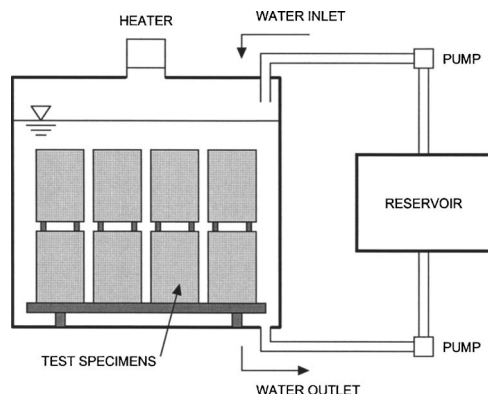


**Fig. 3.** Schematic of wet-dry exposure tank

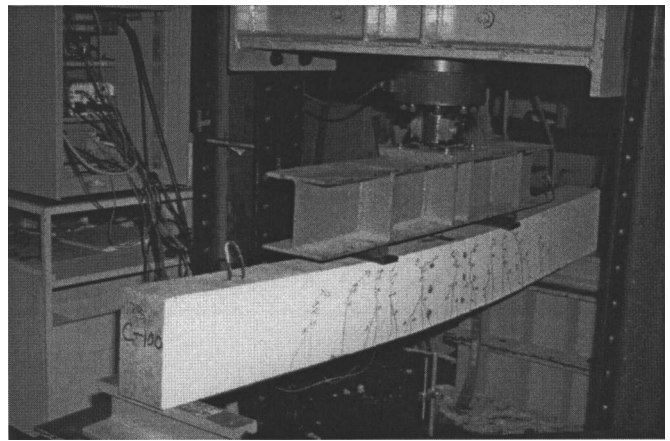


**Fig. 4.** Test setup

### Electrical Potential Measurement

The most practical method of detecting the presence of active corrosion is the measurement of electrical potentials of the reinforcing steel, using a reference half-cell. Theoretically, the corrosion potentials of the reinforcing steel will shift toward the negative direction if the surface of the steel changes from the passive to the active state. Therefore, half-cell potential measurement would imply the possibility of corrosion activity, but does not establish an actual corrosion rate. The measurement procedure is described in the ASTM C 876-80.

In this study, the GalvaPulse device (GP-5000) was used. One wire connection of the GP-5000 was placed on the surface of the test beam with a wet sponge between the concrete surface and the sensor (Fig. 5). The other wire was connected to the exposed reinforcing bar at the end of the beam, thus completing an electrical circuit. The bar was exposed by drilling a hole through the concrete cross section at the end of the beam. After the measurement was taken, the hole was filled with mortar and cycling continued.

For all the beams, half-cell potential readings were taken at seven different locations along the length of the beam as shown in Fig. 6. The half-cell potentials for the CarboDur CFRP strengthened beams are shown in Fig. 7. It can be seen that the corrosion potentials for the beams subjected to 200 and 300 cycles were in the range from  $-300$  to  $-500$  mV, while corrosion potentials of the beams exposed to 100 cycles were in the range from  $-200$  to  $-370$  mV. The corrosion potentials for the control beams were in the range from  $-100$  to  $-250$  mV. According to ASTM C 876-80, measured potentials more positive than  $-200$  mV, represent greater than 90% probability of no active corrosion; potentials between  $-200$  and  $-350$  mV, active corrosion is uncertain; and potentials more negative than  $-350$  mV, there is greater than 90% probability of active corrosion.

Based on the measured potentials, it can be deduced that the active corrosion conditions may have occurred on the reinforcing steel bars in the beams subjected to 200 and 300 cycles. This is reinforced by the visual signs of corrosion observed on the 300 cycle beam. The distribution of the potential values showed more negative values in the central areas of the beams, which implied that those areas could have more active corrosion than the ends of the beam. The beams strengthened by the sheets had more positive corrosion potentials compared to the rest of the beams (including the control beams) and the corrosion state was in the uncertain region. The CFRP sheets and the epoxy resin, applied

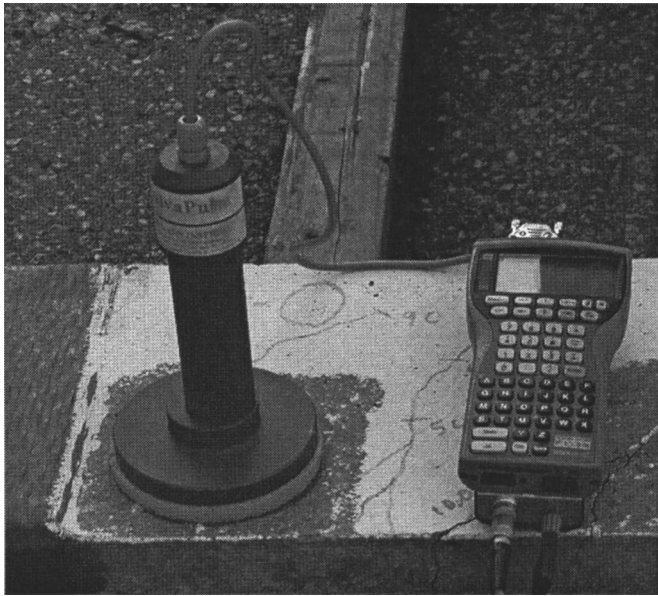


Fig. 5. GalvaPulse device and guard ring

on the surface of the specimens, may have minimized the chloride ionic diffusion and this caused a reduction in the corrosion activity.

### Corrosion Rate Measurements

Corrosion rates were measured using the Galva Pulse GP-5000 device. The GP-5000 determines the corrosion current  $I_{corr}$  from the linear polarization resistance  $R_p$  using the “Stern-Geary” relationship:  $I_{corr} = B/R_p$ , where  $B=26$ . One advantage of the GP-5000 is its ability to confine the area of measurement by the use of a sensor controlled guard ring. The following are broad criteria for the corrosion rate measurements with the sensor controlled guard ring (Broomfield 1993):

- $I_{corr} < 0.1 \mu A/cm^2$  (no corrosion damage expected);
- $0.1 < I_{corr} < 1.0 \mu A/cm^2$  (low to moderate corrosion);
- $1.0 < I_{corr} < 10.0 \mu A/cm^2$  (moderate to high corrosion); and
- $10.0 < I_{corr} < 100.0 \mu A/cm^2$  (high corrosion).

In this study, measurements were taken at the same seven locations on the beam used for the half-cell potential measurements (Fig. 6). The guard ring only covered one main bar in between two stirrups during each measurement. The measurement was taken following the procedure specified by the manufacturer. Before starting a measurement, the surface of the beam was sprayed

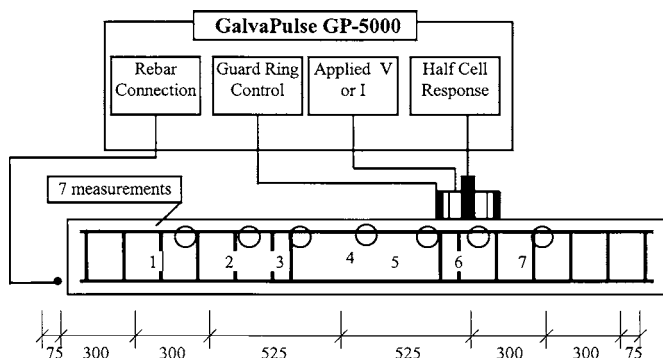


Fig. 6. GalvaPulse connection and corrosion rate measurements

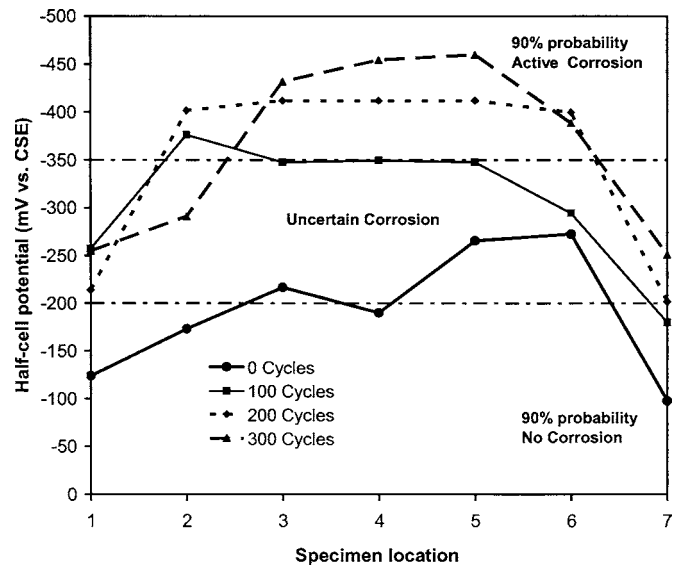


Fig. 7. Half-cell potential measurements—beams strengthened with CarboDur strips

with water (not saturated) and then a wet pad was placed on the measurement location and the sensor was mounted on top. Special attention was paid to ensure good electrical contact between the guard ring and the concrete surface.

For the CarboDur strengthened beams, the measured corrosion rates for the 100, 200, and 300 cycles were 7, 11, and  $12 \mu A/cm^2$ , respectively. For the multiple CFRP sheets/epoxy resin strengthened beams, these values were 3, 5, and  $7 \mu A/cm^2$ , respectively. It is clear that as the number of wet and dry cycles increased, the chloride gradually diffused into the concrete. As a result, the passive state of steel in some areas may no longer exist and the corrosion is induced. After 300 cycles, the measurements indicate high corrosion activity in the beams, which is in agreement with the half-cell potential results. It is also noted that the corrosion rate of the beams with multiple CFRP sheets/epoxy resin is lower than the other beams after 100 cycles. This may indicate that the CFRP sheets minimized chloride ionic diffusion and reduced the corrosion activity.

### Chloride Profiling

To gain an understanding of how the chlorides penetrated the concrete over time, following structural testing, 50 mm diameter cores were drilled through the side of the beam at a location with minimum load-induced cracking. Each core was then cut into 12 disks measuring 12.5 mm thick. The disks were pulverized into a fine powder and mixed in a known amount of distilled water. The water-soluble chloride content in each sample was quantified using an ion chromatograph. The procedure followed ASTM C 1218M-97. Fig. 8 shows the profile of the chlorides in percent mass of cement across the CarboDur strengthened beams for 0 to 300 cycle series. According to Bentur et al. (1997), chloride levels below 0.4% by mass of cement do not pose much of a risk for corrosion. However, chloride levels above 1% by mass of cement may cause rapid deterioration due to corrosion activity. Fig. 8 shows that as the number of cycles increased the chloride levels in the beams increased. Based on the measured chloride profiles, the corrosion risk reaches a medium to high level for the 200 and 300 cycle beams. On the other hand, for the Forca-Tow strengthened beams, where a layer of epoxy was applied to the

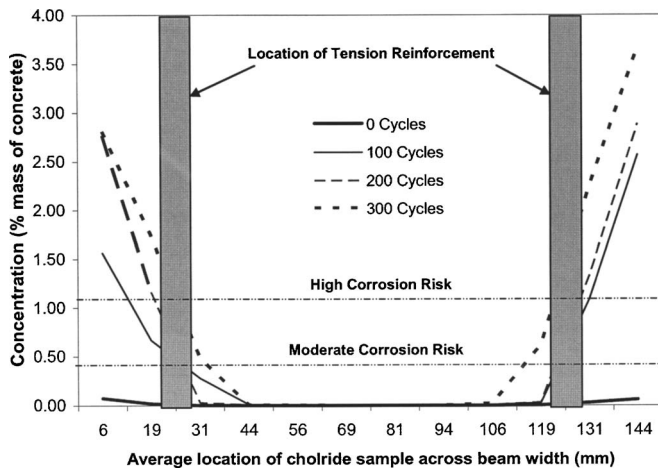


Fig. 8. Chloride profile—beams strengthened with CarboDur strips

surface of the beam (the bottom and the two sides), the internal chloride content was not significant to be quantified. This indicates that the layer of epoxy sealed the surface and minimized the ability of the chlorides to ingress into the concrete up to 300 cycles of exposure.

#### Mass Loss Analysis

Using a diamond tipped saw, sections of rebar were removed from each specimen measuring approximately 250 mm in length. In accordance with ASTM G 1-90, mass loss analysis was performed on the reinforcing steel bars to get the degree of corrosion. Table 3 shows the results for the steel bars extracted from the CarboDur strengthened beams. As expected, the level of corrosion increases with the number of cycles. The initial mass loss at 100 cycles is negligible. This is in agreement with the chloride analysis, which shows that the level of chlorides is below the threshold for this amount of exposure. The corrosion levels at 200 and 300 cycles show that the mass loss is 1 and 1.3%, respectively. Several studies have shown that this level of mass loss is not significant enough to lessen the strength of the beam (Uomoto et al. 1984; Mangat and Elgarf 1999; Badawi and Soudki 2005; El Maaddawy and Soudki 2005; El Maaddawy et al. 2005). The

Table 3. Mass Loss Analysis on CarboDur Series Beams

Number of cycles	Degree of mass loss (%)
0	0.00
100	0.00
200	1.00
300	1.33

reduction in the cross section is minimal, and the bond strength has been shown to actually increase at low levels of corrosion (Soudki and Sherwood 2003). This explains why after exposure there are no visible reductions in strength for the control specimens.

Mass loss analysis on the Forca-Tow strengthened beams indicated that for all cycles, no measurable mass loss occurred. This is consistent with the chloride results and half-cell potential measurements, possibly because the epoxy coating did not allow chlorides to ingress to the steel level.

#### Effect of Wet-Dry Cycles in the Structural Behavior

##### Strengthening Efficiency

The two strengthening schemes were designed to give the same flexural capacity of the strengthened beams taking into account that, at the time of testing, the smallest available size of CFRP CarboDur strips (50 mm width  $\times$  1.2 mm thick) was used. According to the provisions of the ACI 440.2R-02 (2002) and ACI 318-05 (2005), the nominal flexural,  $M_n$ , and shear,  $V_f$ , strengths of the strengthened beams can be calculated using the following equations:

$$M_n = A_s f_s \left( d - \frac{\beta_1 c}{2} \right) + \Psi_f A_f f_{fe} \left( h - \frac{\beta_1 c}{2} \right) \quad (1)$$

$$V_f = (2\sqrt{f_c}) b_w d + \frac{A_{sv} f_y (\sin \alpha + \cos \alpha) d}{s} + \frac{A_{fw} f_{fe} (\sin \alpha + \cos \alpha) d_f}{s_f} \quad (2)$$

Both strengthening schemes give approximately 100% increase in flexural capacity. In addition, due to the use of the

Table 4. Theoretical and Experimental Results

Beam		Ultimate CFRP strain (microns)	Experimental moment (kN m)			$\frac{M_u}{M_0}$	$M_{ACI}$ (kN m)	$V_{ACI}$ (kN)	$\frac{M_u}{M_{ACI}}$	Failure mode
			$M_{cr}$	$M_y$	$M_u$					
Unstrengthened	C-0	—	10.13	19.13	23.83	1.00			1.12	Steel yielding
	C-100	—	9.38	19.13	24.9	1.04	21.2	39.8	1.17	Steel yielding
	C-300	—	8.0	18.38	25.36	1.06			1.20	Steel yielding
CarboDur strips	S-0	10567	13.5	26.25	44.17	1.00			1.03	Rupture
	S-100	7419	13.5	27.00	35.85	0.81	43.0	39.8	0.83	Debonding
	S-200	6193	13.5	24.75	33.30	0.75			0.77	Debonding
	S-300	5784	13.5	23.63	31.91	0.72			0.74	Debonding
Forca-Tow sheets	T-0	9168	13.13	30.00	48.46	1.00			1.07	Debonding
	T-100	8029	13.13	30.00	47.77	0.98	45.2	51.9	1.06	Debonding
	T-200	7571	14.25	28.50	45.53	0.94			1.01	Debonding
	T-300	8418	14.25	28.13	43.31	0.89			0.96	Debonding

Note:  $M_{ACI}$  and  $V_{ACI}$  = the flexural and shear strengths, respectively, calculated according to ACI 440.2R-02;  $M_{cr}$  = cracking moment;  $M_y$  = yield moment;  $M_u$  = ultimate moment;  $M_0$  = ultimate moment at 0 cycles for each group.

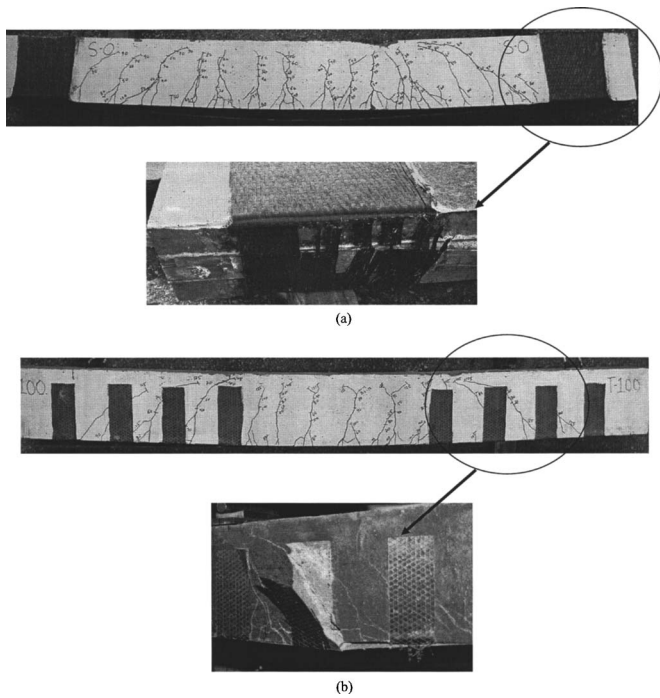


**Fig. 9.** Mode of failure: (a) beams strengthened with CarboDur strips; (b) beams strengthened with Forca-Tow sheets

transverse U-shaped Forca-Tow CFRP straps, Scheme II gives an approximate 30% increase in shear (Table 4). The experimental results are in very good agreement with the ACI code predictions, especially those for the unconditioned (control) beams.

The final cracking patterns and modes of failure for CFRP strengthened beams are shown in Figs. 9(a and b) for the CarboDur and Forca-Tow strengthening schemes, respectively. Fig. 10 graphically illustrates the effectiveness of the CFRP strengthening and compares the behavior of unexposed beams C-0, S-0, and T-0 that were not subjected to any wet-dry cycles. The load-deflection graphs in Fig. 10 show clearly that all CFRP strengthened beams performed significantly better than their control (unstrengthened) counterparts, both in terms of strength and postyield stiffness. The beams tested were lightly reinforced with steel reinforcement and,

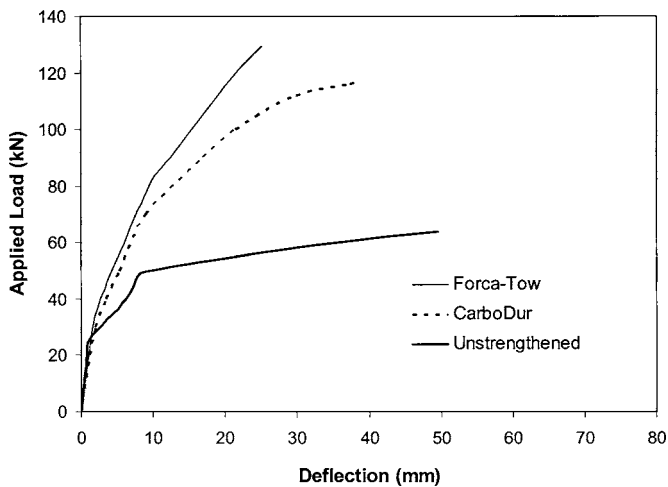


**Fig. 10.** Load-deflection relationship for strengthened and unstrengthened beams (at 0 cycle)

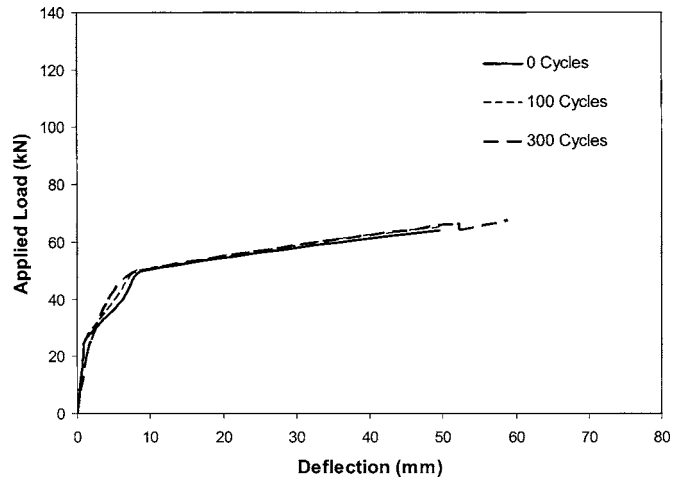


**Fig. 11.** Load-deflection relationship for unstrengthened (control) beams

hence, the CFRP strengthening has a significant effect. Table 4 gives the experimental values of the cracking and failure moments for the tested beams. The load carrying capacity of the strengthened beams increased by 97% (CarboDur strips) to 115% (Forca-Tow Sheets), while the maximum deflection, at failure, decreased by 21% (CarboDur strips) to 42% (Forca-Tow Sheets). There was a significant enhancement in the postcracking stiffness for the strengthened compared to unstrengthened beams.

#### Unstrengthened Beams

All unstrengthened control beams failed by yielding of steel tension reinforcement followed by crushing of the concrete directly under one of the applied concentrated loads. Fig. 11 shows the load-midspan deflection curves for the unstrengthened beams subjected to 0, 100, and 300 cycles. The load-deflection characteristics for the three beams are very similar and their behavior is typical of under-reinforced beams with failure loads within 5% of the theoretical values. No significant effect of the wet-dry cycles was observed. This implies that the corrosion has not reached a significant level to affect the structural performance of the beams by means of reinforcing steel mass loss or bond degradation. This is confirmed by the destructive and nondestructive tests discussed earlier. Further studies should include higher level of exposure, more than 300 cycles.

#### Beams Strengthened with CFRP Strips

All beams of this group, except S-0, had premature failures by debonding of the CFRP strips. The debonding started at the plate ends and then spread over the whole length of the beam. For beam S-0, which was kept at room temperature, the failure was by rupture of the CFRP plate at the midspan. It is worth mentioning here that the maximum reported strain in the CFRP strips for beam S-0 was 1.057% (Table 4), which is less than the rupture strain of 1.7%, were measured at approximately 90% of the failure load. Fig. 12 shows the load-deflection behavior for the beams of this group. For all beams except S-0, it can be seen that after the debonding of the strips, the load capacities dropped instantaneously and closely followed the load deflection of the unstrengthened beams. The beam S-0 carried 25% to 45% more load and had 32% to 68% more strain than its counterpart beams which were exposed to wet-dry cycles. The effect of wet-dry cycles was to decrease the maximum loads by reducing the bond

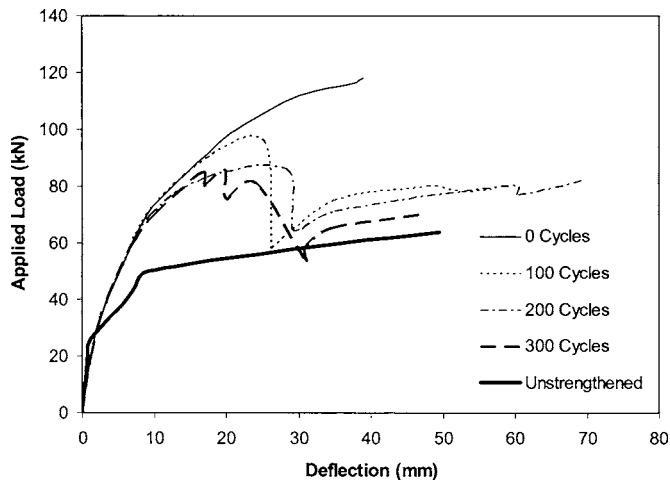


**Fig. 12.** Load-deflection relationship for beams strengthened with CarboDur strips

at the interface between the CFRP plate and the concrete causing the premature failure (Table 4). Interfacial bond strength is dependent on the shear strength of the concrete cover and the epoxy adhesive, which were possibly degraded by the wet-dry cycling. The reduction in load was 19, 25, and 28% after 100, 200, and 300 cycles, respectively. The lower value of maximum measured CFRP plate strain with the increased number of cycles suggest that a slip, or relative displacement of the CFRP plate to concrete surface, has occurred (Fig. 12). The use of moisture epoxy adhesive will improve the durability aspect and enhance the bond transfer for beams strengthened with CFRP sheets.

#### Beams Strengthened with CFRP Sheets

Fig. 13 shows the load-deflection relationship for the beams strengthened with CFRP sheets. All beams of this group failed by delamination of the sheets. The postdelamination behavior was similar to the after-debonding one of the beams strengthened with the strips. The failure started by delamination and ruptures of transverse U-shaped wraps and followed by delamination of the longitudinal flexural sheets. The wet-dry cycles had a small effect on the strength of the beams of this group (Table 4). The reduc-

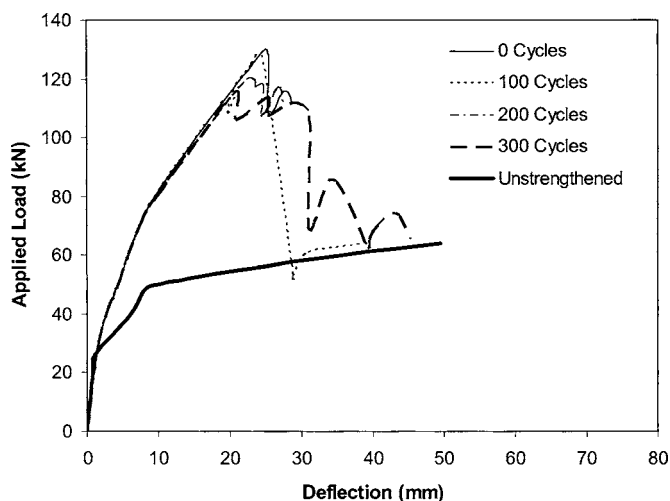


**Fig. 13.** Load-deflection relationship for beams strengthened with Forca-Tow sheets

tion in maximum load was 2, 6, and 11% after 100, 200, and 300 cycles, respectively. That was expected due to the epoxy resin, which covered both sides and the bottom of the beams, and is in agreement with the results of the corrosion activity.

## Conclusions

This paper presented the results of an experimental program investigating the durability and behavior of concrete beams strengthened with CFRP sheets subjected to a corrosive environment. Based on the test results, the following can be concluded:

1. CFRP strengthening significantly enhanced the performance of RC beams with the load capacity of almost double that of unstrengthened specimens;
2. Corrosion rates and half-cell potentials indicated high corrosion activity after 200 cycles, while minimal corrosion activity detected up to 100 cycles. Visible corrosion cracking and staining appeared after 300 wet/dry cycles;
3. Chloride profiling and mass loss analysis agreed with the nondestructive tests showing that critical chloride levels had reached the reinforcing bars at 200 cycles, and the corrosion process of reinforcing bars was in progress;
4. CFRP sheets and the resin system appeared to decrease chloride ionic diffusion and may reduce the corrosion rate of reinforcing steel in the beams;
5. The ultimate capacity of the CFRP strengthened beams decreased by 11 to 28% over 300 cycles. The stiffness and yield load was not affected by the environmental exposure; and
6. Failure mode for a beam strengthened with CFRP strips was by debonding of the strips and the time to delaminate was shortened by increased wet-dry cycles.

## Acknowledgments

The research was conducted with the financial assistance of Materials Manufacturing Ontario and the Natural Sciences and Engineering Research Council. The CarboDur system was donated by Sika Canada, and the Forca-Tow strengthening system was partially supported by ISIS Canada Network of Centres of Excellence. Thanks are extended to the technical staff at the Civil Engineering Department, University of Waterloo for their assistance during various stages of the work.

## Notation

The following symbols are used in the paper:

- $A_f$  = area of FRP external reinforcement,  $\text{mm}^2$ ;
- $A_{fv}$  = area of FRP shear reinforcement with spacing  $s_f$ ,  $\text{mm}^2$ ;
- $A_s$  = area of steel reinforcement,  $\text{mm}^2$ ;
- $A_{sv}$  = area of steel shear reinforcement with spacing  $s$ ,  $\text{mm}^2$ ;
- $b_w$  = web width, mm;
- $c$  = distance from extreme compression fiber to the neutral axis, mm;
- $d$  = depth of steel reinforcement, mm;
- $d_f$  = depth of FRP shear reinforcement, mm;
- $f'_c$  = compressive strength of concrete, MPa;

$f_{fe}$  = effective stress in the FRP; stress level attained at section failure, MPa;  
 $f_s$  = stress in steel bars, MPa;  
 $f_y$  = yield strength of steel reinforcing bars, MPa;  
 $h$  = overall thickness of a member, mm;  
 $M_n$  = nominal flexural strength, kN m;  
 $V_f$  = nominal shear strength, kN;  
 $s$  = spacing of steel shear reinforcement;  
 $s_f$  = spacing of FRP shear reinforcement;  
 $\alpha$  = angle of inclination of stirrups, degrees;  
 $\beta_1$  = ratio of depth of the equivalent rectangular stress block to the depth of the neutral axis; and  
 $\Psi_f$  = additional FRP-strength-reduction factor (taken equals to 1.0 for this study).

## References

- ACI Committee 318. (2005). "Building code requirements for structural concrete and commentary." *ACI 318-05/318R-05*, American Concrete Institute, Farmington Hills, Mich.
- ACI Committee 440. (2002). "Guide for the design and construction of externally bonded FRP systems for strengthening concrete structures." *ACI 440.2R-02*, American Concrete Institute, Farmington Hills, Mich.
- Badawi, M., and Soudki, K. (2005). "Control of corrosion-induced damage in reinforced concrete beams using carbon fiber-reinforced polymer laminates." *J. Compos. Constr.*, 9(2), 195–201.
- Bentur, A., Diamond, S., and Berke, N. S. (1997). "Steel corrosion in concrete." E & FN Spon, London.
- Broomfield, J. E., Rodriguez, J., Ortega, L. M., and Garcia, A. M. (1993). "Corrosion rate measurement and life prediction for reinforced concrete structures." *Proc., Structural Faults and Repair-93*, Univ. of Edinburgh, Scotland, Vol. 2, 155–164.
- Chajes, M. J., Thomson, T. A., and Farschman, C. A. (1995). "Durability of concrete beams externally reinforced with composite fabrics." *Constr. Build. Mater.*, 9(3), 141–148.
- El Maaddawy, T., and Soudki, K. (2005). "Carbon-fiber-reinforced polymer repair to extend service life of corroded reinforced concrete beams." *J. Compos. Constr.*, 9(2), 187–194.
- El Maaddawy, T., Soudki, K., and Topper, T. (2005). "Computer-based mathematical model for performance prediction of corroded beams repaired with fiber reinforced polymers." *J. Compos. Constr.*, 9(3), 227–235.
- Mangat, P. S., and Elgarf, M. S. (1999). "Flexural strength of concrete beams with corroding reinforcement." *ACI Struct. J.*, 96(1), 149–158.
- Matthys, S. (2000). "Structural behavior and design of concrete members strengthened with externally bonded FRP reinforcement." Ph.D. dissertation, Dept. of Structural Engineering, Faculty of Applied Science, Ghent Univ., Belgium.
- Mohammed, T., Otsuki, N., and Hamada, H. (2003). "Corrosion of steel bars in cracked concrete under marine environment." *J. Mater. Civ. Eng.*, 15(5), 460–469.
- Neale, K. W. (2000). "FRPs for structural rehabilitation: A survey of recent progress." *Prog. Struct. Eng. Mater.*, 2(2), 133–138.
- Soudki, K., and Sherwood, T. (2003). "Bond behavior of corroded steel reinforcement in concrete wrapped with carbon fiber reinforced polymer sheets." *J. Mater. Civ. Eng.*, 15(4), 358–370.
- Spadea, G., Bencardino, F., and Swamy, R. (1998). "Structural behavior of composite RC beams with externally bonded CFRP." *J. Compos. Constr.*, 2(3), 132–137.
- Spainhour, L. K., and Thompson, I. (1998). "Effect of carbon fibre jackets on reinforced concrete columns exposed to a simulated tidal zone." *Proc., 2nd Int. Conf. on Composites in Infrastructure*, H. Saadatmanesh and M. R. Ehsani, eds., Tucson, Ariz., Vol. 1.
- Tamuzs, V., and Tepfers, R. (2004). "Strengthening of concrete structures with advanced composite materials: Prospects and problems." *J. Mater. Civ. Eng.*, 16(5), 391–397.
- Toutanji, H., and Balaguru, P. (1998). "Durability characteristics of concrete columns wrapped with fiber tow sheets." *J. Mater. Civ. Eng.*, 10(1), 52–57.
- Triantafillou, T. C. (1998). "Strengthening of structures with advanced FRPs." *Prog. Struct. Eng. Mater.*, 1, 126–134.
- Uomoto, T., Tsuji, K., and Kakizawa, T. (1984). "Deterioration mechanism of concrete structures caused by corrosion of reinforcing bars." *Trans. Jpn. Concr. Inst.*, 6, 163–170.